Metadata of the chapter that will be visualized online

Chapter Title	From Macroelectrodes to Microelectrodes: Theory and Electrode Properties	
Copyright Year	2014	
Copyright Holder	Springer Science+Business Media New York	
Corresponding Author	Family Name	**Daniele**
	Particle	
	Given Name	**Salvatore**
	Suffix	
	Division	Department of Molecular Sciences and Nanosystems
	Organization	University Ca' Foscari of Venice
	Address	Calle Larga S. Marta, Dorsoduro 2137, 30123 Venice, Italy
	Email	sig@unive.it
Author	Family Name	**Bragato**
	Particle	
	Given Name	**Carlo**
	Suffix	
	Division	Department of Molecular Sciences and Nanosystems
	Organization	University Ca' Foscari of Venice
	Address	Calle Larga S. Marta, Dorsoduro 2137, 30123 Venice, Italy
Abstract	Voltammetry involves the application of a potential that varies with time and the measurement of a current that flows between a working and a reference electrode. Voltammetry can therefore be defined as the exploration of the three-dimensional space that relates to potential, current, and time.1 However, under suitable circumstances, simplified conditions can lead to a unique relation, not involving time, between current and potential; such situation provides the so-called steady-state voltammetry.2	

Chapter 15
From Macroelectrodes to Microelectrodes: Theory and Electrode Properties

Salvatore Daniele and Carlo Bragato

15.1 Introduction

15.1.1 Voltammetry: A Brief History

Voltammetry involves the application of a potential that varies with time and the measurement of a current that flows between a working and a reference electrode. Voltammetry can therefore be defined as the exploration of the three-dimensional space that relates to potential, current, and time.[1] However, under suitable circumstances, simplified conditions can lead to a unique relation, not involving time, between current and potential; such situation provides the so-called steady-state voltammetry.[2]

Voltammetric techniques date back to the early of nineteenth century, following the experiments made by Heyrovsky in 1922, and when, for the first time, he showed that by measuring the current while the potential of a dropping mercury electrode (DME) was changed, it was possible to obtain information on the nature of the species in the solution that were reduced at the electrode surface. This technique, called polarography, was used for analytical applications, especially of metal ions. The term voltammetry was first introduced in 1940 to describe experiments, similar to those made at a DME, performed at a solid working electrode.[1] Many variations of the basic polarography were developed during the 1940s and early 1950s. Pulsed waveforms in conjunction with DMEs or static mercury electrodes have been developed and largely applied for analytical investigations.[1] The pulsed techniques were aimed at decreasing the contribution of the capacitive current, which originates from charging the electrical double-layer capacitance that exists at the interface between the electrode and the solution. The charging current

S. Daniele (✉) • C. Bragato
Department of Molecular Sciences and Nanosystems, University Ca' Foscari of Venice, Calle Larga S. Marta, Dorsoduro 2137, 30123 Venice, Italy
e-mail: sig@unive.it

AU1

L. Moretto, K. Kalcher (eds.), *Environmental Analysis by Electrochemical Sensors and Biosensors*, DOI 10.1007/978-1-4939-0676-5_15

is non-faradaic and produces baseline current that must be subtracted in voltammetric measurements to improve the sensitivity, especially for trace species analysis.[3]

A further impetus in the development of voltammetric techniques has been recorded during the 1980s with the advent of much smaller, than previously employed, electrodes, which were of millimeter size. The smaller electrodes have micrometer size and are commonly referred to as either ultramicroelectrodes (UMEs) or, simply, microelectrodes (MEs).[4–13] Since then, the field of MEs has generated enormous excitement and has seen a huge increase in popularity with the rapid developments in nanofabrication capable of preparing well-defined electrodes of sub-micrometer size down to a few nanometers.[14, 15] Such very small electrodes are nowadays defined nanoelectrodes (NEs). The latter category, normally, includes all electrodes that possess at least one dimension less than 100 nm.[15] It must be considered that the main properties of both MEs and NEs come from a common operational characteristic. It involves the circumstance that under given experimental conditions, the diffusion layer thickness is thicker than the characteristic length of the electrode.[12]

This chapter is concerned with methods in which a constant potential or a potential varied with time is applied to either millimeter sized (called conventional electrodes) or MEs and the ensuing current response as a function of time or potential is measured.

15.2 Mass Transport and Electrode Geometry

A typical electrode reaction involves the transfer of charge between an electrode and a species in solution. The whole process involves a series of steps, including the rate of the electron transfer at the electrode surface and the movement of reactant in and out of the interface, that is, the mass transport within the solution. Both phenomena are important in predicting the current flowing in the electrochemical cell. The model of the electrode kinetics predicts that the rate of the electron transfer is affected by the electrode voltage through an exponential relationship.[3] The current therefore, over a potential region, also increases exponentially by increasing the electrode potential. The current increase is limited by the mass transport of both reactant and electrode reaction product (see Chap 10 for details). AU2

There are three forms of mass transport which can influence an electrolysis process:

- Diffusion
- Convection
- Migration

Diffusion occurs in all solutions and arises from local uneven concentrations of reagents. It is particularly significant in an electrolysis experiment since the conversion reaction only occurs at the electrode surface. Consequently, there will be a

lower reactant concentration at the electrode than in bulk solution. Similarly, a higher concentration of product will exist near to the electrode than further out into the solution.

Convection originates from the action of a force on the solution. There are two forms of convection. The first is termed *natural convection* and is present in any solution. This natural convection is generated by small thermal or density differences and acts to mix the solution in a random and therefore unpredictable manner. In the case of electrochemical measurements, these effects tend to cause problems if the measurement time for the experiment exceeds 20 s.[3] The second type is termed *forced convection*. It is typically several orders of magnitude greater than any natural convection and therefore effectively removes the random aspect, due to natural convection, from the experimental measurements. This of course is only true if the convection is introduced in a well-defined and quantitative manner.[3]

Migration is essentially an electrostatic effect which arises due the application of a voltage at the electrodes. Any charged species near that interface will either be attracted or repelled from it by electrostatic forces.

Due to ion solvation effects and diffuse layer interactions in solution, migration is usually difficult to calculate accurately for real solutions. Most electrochemical measurements, therefore, are performed in solutions which contain a background electrolyte that does not undergo electrolysis itself but helps to shield the reactants from migratory effects. By adding a large quantity of the electrolyte (relative to the reactants), it is possible to ensure that the electrolysis reaction is not significantly effected by migration.

On the above basis, it is evident that to gain a quantitative model of the current flowing at the electrode, one must account for the electrode kinetics, the three-dimensional diffusion, convection, and migration contributions of all the species involved.

The total mass transport of a given species i is given by the flux, J_i (mol s^{-1} cm^{-2}), to an electrode and is described by the Nernst-Planck equation[3]:

$$J_i = -D_i \nabla C_i - \frac{Z_i F}{RT} D_i C_i \nabla \phi + v C_i \qquad (15.1)$$

The flux is related to the current through

$$J_i = \frac{i}{nFA} \qquad (15.2)$$

The solution of Eq. (15.1) is difficult to solve and currently is beyond the capacity of even the fastest computers. However, electrochemical experiments can be designed to eliminate the contributions of electrostatic potential and hydrodynamic velocity to the overall flux of electroactive species, limiting mass transport to the contribution from *diffusion*. The currents resulting from these experiments can then be classified as *diffusion controlled*.[3]

Table 15.1 Diffusion equations for different electrode geometries

Electrode geometry	Diffusion equation	
Planar	$\frac{\partial c}{\partial t} = D\left(\frac{\partial^2 c}{\partial x^2}\right)$	$T_{1,1}$
Sphere, hemisphere	$\frac{\partial c}{\partial t} = D\left(\frac{\partial^2 c}{\partial r^2} + \frac{2}{r}\frac{\partial c}{\partial r}\right)$	$T_{1,2}$
Cylinder	$\frac{\partial c}{\partial t} = D\left(\frac{\partial^2 c}{\partial r^2} + \frac{1}{r}\frac{\partial c}{\partial r}\right)$	$T_{1,3}$
Microdisk	$\frac{\partial c}{\partial t} = D\left(\frac{\partial^2 c}{\partial r^2} + \frac{1}{r}\frac{\partial c}{\partial r} + \frac{\partial^2 c}{\partial z^2}\right)$	$T_{1,4}$
Band	$\frac{\partial c}{\partial t} = D\left(\frac{\partial^2 c}{\partial x^2} + \frac{\partial^2 c}{\partial z^2}\right)$	$T_{1,5}$

Contributions from migration can be effectively eliminated by adding an inert electrolyte to the solution at a 10–100-fold excess with respect to the redox couple of interest. The electric field between the two electrodes involved in the measurement is dissipated over all of the ions in solution and not just the electroactive material. Under these conditions, the contribution of migration to the observed current is <1 %. Contributions from convection can be reduced or eliminated by working in quiescent solutions. With careful control of external vibration and temperature, diffusion controlled measurements for up to 20 s or close can be made without significant convective effects.[3]

In the following section how the diffusion mass transport will control the current at electrodes of different sizes and geometries will be described.

15.2.1 Diffusion Equations and Current Responses

Fick's first and second laws describe the flux of a species and its concentration as functions of time and position, respectively. The general formulations of Fick's laws for the species O at any geometry are:

$$J_O = -D_O \nabla C_O \tag{15.3}$$

$$\frac{\partial C_O}{\partial t} = D_O \nabla^2 C_O \tag{15.4}$$

Although the diffusion equations require, in general, three spatial coordinates to describe the mass transport, in the cases of an infinite plane, a sphere, and an infinitely long cylinder, the boundary allows a reduction from three to one of the number of spatial coordinates. These geometries simplify the Laplace operator so that Eqs. (15.3) and (15.4) acquire simpler forms. The concentration gradient at the electrode surface is obtained by solving Fick's second law, and Table 15.1 shows the simplified forms of the diffusion equations for such electrode geometries. For planar diffusion x is the spatial coordinate directed to the boundary ad having its origin at the boundary surface (Fig. 15.1a). In the case of spherical (Fig. 15.1b) and cylindrical geometries, r represents the radial distance from the electrode center. The solution of these equations, under appropriate boundary conditions, yields the

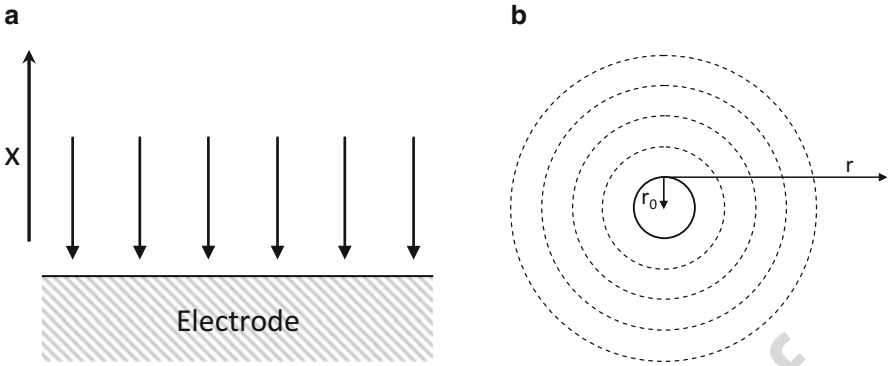

Fig. 15.1 Diffusion mass transport to: (**a**) planar electrode; (**b**) spherical electrode

concentration profiles, $C(x,t)$, i.e., the change of concentration of that species as functions of the distance and time. Boundary conditions, in turn, depend on the electrochemical experiments performed.

15.2.2 Application of a Potential Step

The experiment of interest involves stepping the potential from an initial value, where no electrode reaction occurs, to one at which electrolysis proceeds at diffusion controlled rate. The general reaction considered is:

$$O + ne \leftrightarrows R \tag{15.5}$$

and the electrode is placed in a semi-infinite solution containing only the electroactive species O of concentration C_O^*. The semi-infinite condition highlights the fact the volume of the electrolytic solution is much larger than the electrode size. It is also assumed that a sufficient negative potential is applied at the working electrode so that the surface concentration of O becomes equal to zero, regardless of whether the kinetics of the process is facile or sluggish. Examples of boundary conditions, which are valid under the electrochemical experiment outlined above, are

$$\begin{array}{lll} C_O(x,0) = C_O* & (\text{for all } x) & \text{Initial conditions} \\ C_R(x,0) = 0 & (\text{for all } x) & \text{Initial conditions} \\ \lim\limits_{x\to\infty} C_0(x,t) = C_O^* & (\text{at all } t) & \text{Semi-infinite conditions} \\ \lim\limits_{x\to\infty} C_R(x,t) = C_R^* & (\text{at all } t) & \text{Semi-infinite conditions} \end{array}$$

Equations for planar (T1,1 in Table 15.1) and spherical (T1,2 in Table 15.1) electrodes can be solved using the Laplace transform technique to give, after considering Eq. (15.2), the time evolution of the current (i_t).

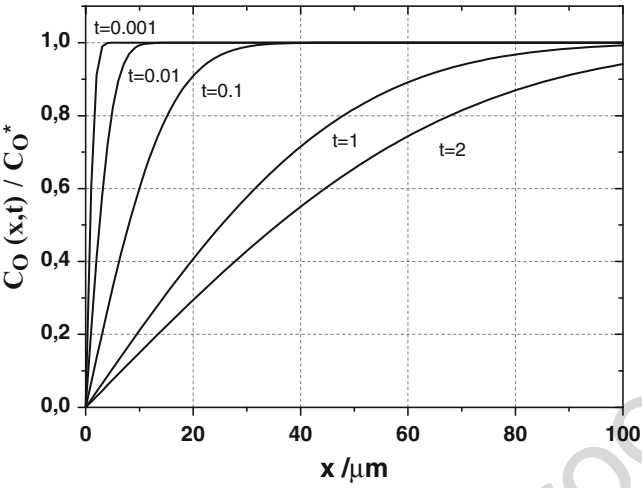

Fig. 15.2 Concentration profiles for a potential step experiments at different step times. Calculations refer to a species having $D_O = 7 \times 10^{-6}$ cm^2 s^{-1}

For a planar electrode, the solution is known as the Cottrell equation and predicts that the current is inversely proportional to $t^{1/2}$

$$i_t = \frac{nFAD_o^{\frac{1}{2}} \cdot C_O^*}{\pi^{\frac{1}{2}} t^{\frac{1}{2}}} \tag{15.6}$$

The reason for the current decay can be explained considering how the concentration profile of the reagent species, near to the electrode surface, varies with time. The concentration profiles are given by

$$C_O(x,t) = C_0^* erf\left[\frac{x}{2\sqrt{D_0 t}}\right] \tag{15.7}$$

where *erf* is the error function. Figure 15.2 displays several plots of the normalized concentration C_O/C^* against distance for various times. It is evident that in the zone near the electrode, the concentration differs from that in the bulk and approaches the latter value asymptotically. It occurs at a distance from the electrode surface, which is defined diffusion layer thickness (δ). As is also evident from Fig. 15.2, δ spreads gradually into the solution as the time increases; the concentration gradient at the electrode surface decreases and overall the current decreases as the time lapses and, theoretically, falls to zero for $t \to \infty$.

The distance at which the species O can diffuse in time t can be predicted by $\delta = (D_O\, t)^{1/2}$ [1] and the distance from the electrode at which the diffusion layer thickness is completely contained is within about $6(D_O\, t)^{1/2}$.[3]

[1] In the literature, δ is also estimated as $(2D_O t)^{1/2}$ and $(\pi D_O t)^{1/2}$.

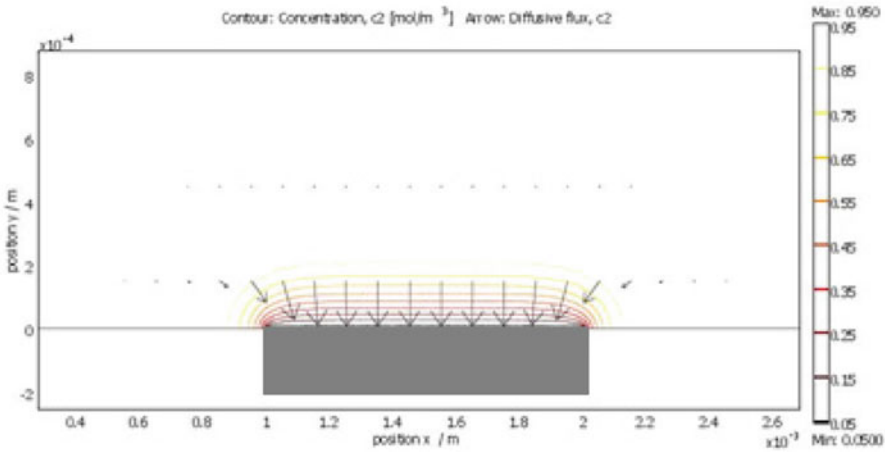

Fig. 15.3 Diffusion flux and concentration profiles at a conventional disk electrode 2 mm diameter. Simulated by the use of COMSOL Multiphysics 3.5 AU8

The conditions for planar diffusion are theoretically fulfilled only if the electrode surface is very large. In case of finite disk electrodes, edge effects arise and linear diffusion is no longer linear overall the electrode surface (Fig. 15.3). Diffusion also develops parallel to the electrode surface in the radial direction. However, if the radius of the disk electrode is large enough with respect to the diffusion layer thickness (as is the case of common employed disk electrode of millimeter size), edge effects can be neglected and Cottrell equation accurately accounts for the current profile at the electrode surface. These electrodes are nowadays called either conventional or macroelectrodes.[3–12]

Returning to a spherical electrode, the solution of the diffusion equation T1,2 provides[3]

$$i(t) = \frac{nFAC_O^b\sqrt{D_O}}{\sqrt{\pi \cdot t}} + \frac{nFAD_OC_O^b}{r_0} \tag{15.8}$$

which contains both a time-dependent term and a time-independent term. Thus, contrary to the planar electrode, the diffusion current at a spherical electrode approaches a constant value for $t \to 0$. The time-dependent term is prevailing at short times, where the constant term contributes negligibly to the overall current, and Eq. (15.8) reduces to the Cottrell relationship (15.6). At long times, the transient term has decayed to a negligible value and the overall current is steady state and is given by the equation:

$$i = 4\pi nFD_oC_o^*r_o \tag{15.9}$$

The reason for such behavior can be understood by considering the concentration profile that establishes to the surface of a sphere given by[3]

$$C_O(r,t) = C_O^* \left[1 - \frac{r_0}{r} erfc \left(\frac{r - r_0}{2\sqrt{D_O \cdot t}} \right) \right] \tag{15.10}$$

The main difference between the latter and Eq. (15.7) is the factor r_0/r, while $(r-r_0)$ is the distance from the electrode surface, similar to x for a planar electrode. When the diffusion layer is very thin, r is small compared to r_0 ; the linear and spherical diffusion situations are practically indistinguishable. On the other hand, when the diffusion layer grows and becomes much larger than r_0 (i.e., $(r-r_0) \ll 2(D_O t)^{1/2}$), it can be shown that the concentration profile is given by[3]

$$C_O(r,t) = C_O^*(1 - r_0/r)$$

and the concentration gradient at the electrode surface is proportional to C_O^*/r_0; this provides the steady-state current.

From a practical point of view, the use of Eq. (15.8), or one of its limiting forms, depends on the electrode size. In fact, linear diffusion describes adequately the mass transport at the electrode surface provided that the radius of the sphere is large enough and the time is relatively short. If, for instance, we consider the case of a hanging mercury electrode (i.e., an almost spherical electrode) 0.1 cm radius, immersed in a solution containing an electroactive species having a diffusion coefficient value of 1×10^{-5} cm^2 s^{-1}, Cottrell equation predicts, with 10 % accuracy, the current recorded within 3 s. For longer electrolysis times, the steady-state term starts to contribute significantly. Instead, the prevailing of the steady-state term for such large electrode would require much longer times, so that natural convection would prevent its fully achievement.[3] The achievement of both short-time and long-time limits at spherical electrodes is made possible with the use of MEs (*vide infra*).

The third type of electrode that involves only a single dimension of diffusion is the cylindrical electrode, and the diffusion equation is shown in Table 15.1 (equation T1,3). Practical electrodes with such a geometry are made by fine metal or carbon wires connected to a conducting bigger wire with silver epoxy.[3, 8–11] Their behavior, therefore, falls within the category of MEs. Theoretical relationships for predicting current responses at such geometry will be considered in more detail in the MEs section.

AU9

15.2.3 *Linear Sweep (LSV) and Cyclic Voltammetry (CV)*

In voltammetry, the potential changes linearly with time (Fig. 15.4a), starting from an initial potential E_i (usually, where no electrode reaction occurs). Eventually, after reaching a potential E_λ, the sweep is reversed and the potential returns linearly to its initial value (Fig. 15.4b). Thus, in LSV or in the forward scan in CV, the potential at any time is given by $E(t) = E_i \pm v\,t$, where v is the sweep rate (or scan

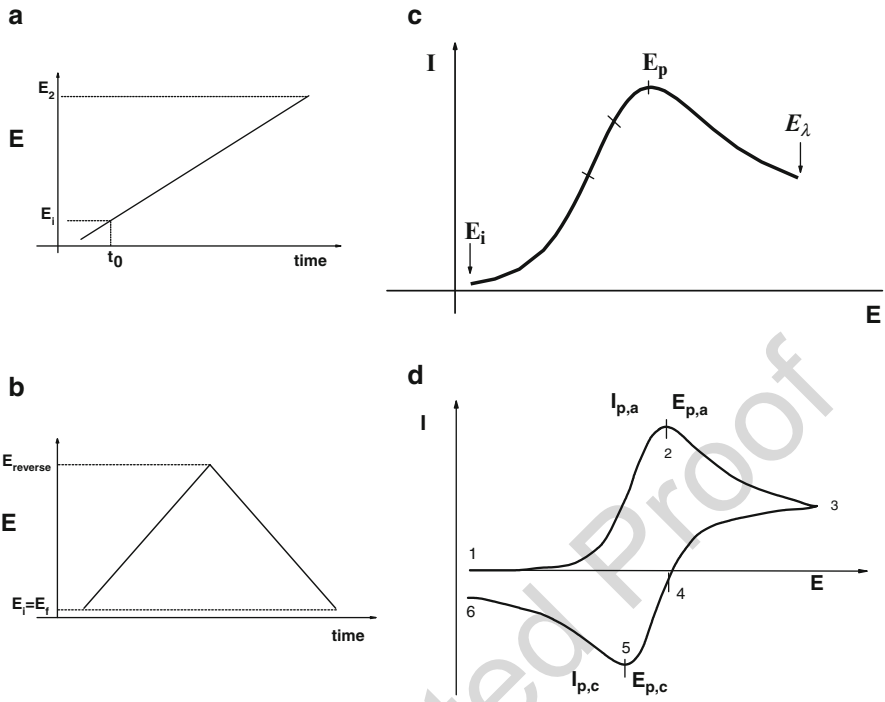

Fig. 15.4 Waveforms for (**a**) LSV and (**b**) CV; current against potential profiles for (**c**) LSV and (**d**) CV (for an oxidation process)

rate) in V s^{-1}. The experiment is considered for reaction (15.5), and it is assumed to be Nernstian (i.e., reversible) in character. For planar and spherical electrodes, the solution of the diffusion equations T1,1 and T1,2, with the appropriate boundary conditions and the applications of numerical methods,[3] provides the Eqs. (15.11) and (15.12), respectively:

$$i = nFAC_O^b(\pi D_O\sigma)^{1/2}\chi(\sigma \cdot t) \tag{15.11}$$

$$i = nFAC_O^b(\pi D_O\sigma)^{1/2}\chi(\sigma \cdot t) + \frac{nFAD_OC_O^*\phi(\sigma t)}{r_0} \tag{15.12}$$

where:

$\sigma = \left(\frac{nF}{RT}\right)v$; $\chi(\sigma \cdot t)$ and $\phi(\sigma t)$ are tabulated values.[3]

Equation (15.11) indicates that the current depends on $v^{1/2}$ (and consequently on time) in case of the planar electrode; whereas, again, for the spherical electrode, there are two terms: the first is the same as for the planar electrode and the second represents the spherical correction. For conventional spherical electrodes (i.e., hanging mercury electrodes) and values of v relatively large, the planar contribution is much larger than the spherical correction. Under these conditions the spherical

electrode can be consider planar. The current against potential curves for such cases under LSV and CV conditions is shown in Fig. 15.4, which displays the typical peak-shaped profiles both for the forward and backward scans.

The peak current of the LSV (or that of the forward scan in CV) is given by:

$$i_p = 0.4463\left(\frac{F^3}{RT}\right)^{1/2} n^{3/2} A D_O^{1/2} C_O^b v^{1/2} \tag{15.13}$$

and the backward (i_{pc}) to forward (i_{pa}) peak current ratio, i_{pc}/i_{pa}, is equal to 1 for a Nernstian wave with a stable product.

15.3 Diffusion at MEs

Microelectrodes, as mentioned in Introduction, are electrodes with characteristic dimensions on the micrometer or sub-micrometer scale.[4–15] An operational definition of ME has been recommended by IUPAC in 2000s in Pure and Applied Chemistry.[12] Practically, it includes any electrode with at least a linear dimension, called critical dimension, that falls in the micrometer and sub-micrometer size. Thus, microelectrodes can be of different geometries, and Fig. 15.5 shows schemes of some of those for which theoretical treatment exists and equations of current as a function of time or potential have been derived.

The experiments using MEs are similar to those described above in the previous section, which essentially hold for conventional or millimeter-sized electrodes. However, as an electrode is miniaturized to micrometer or even sub-micrometer size, semi-infinite planar diffusion gradually transforms into semi-infinite radial diffusion (Fig. 15.6). Longer experiments produce the same phenomenon. Because of the time-dependent change of the diffusion profile, the solid angle developed by the diffusion layer in front of the electrode increases and grows considerably relative to the electrode surface. For this reason, more electroactive species per unit of time and area reach the electrode surface with respect to the planar electrode. Moreover, the flux in and out of the volume eventually becomes stationary and the diffusion layer stops growing. This implies the achievement of a steady-state current at long times.[4–15] The time needed to reach a steady state depends, however, on the geometry and size of the microelectrode. The time needed to reach a steady state depends however on the geometry and size of the microelectrode. AU10

From the above qualitative considerations, it appears that the mass transport to microelectrodes, apart from a few cases, is complicated theoretically, and in the next sections, we describe the current-time and current-potential equations, which have been derived by using either analytical solutions or simulation procedures for MEs having the geometries depicted in the scheme of Fig. 15.5, which have been largely employed for practical applications. Detailed information on how ME or NE can be fabricated can be found in several reports and reviews.[9, 10, 13–16]

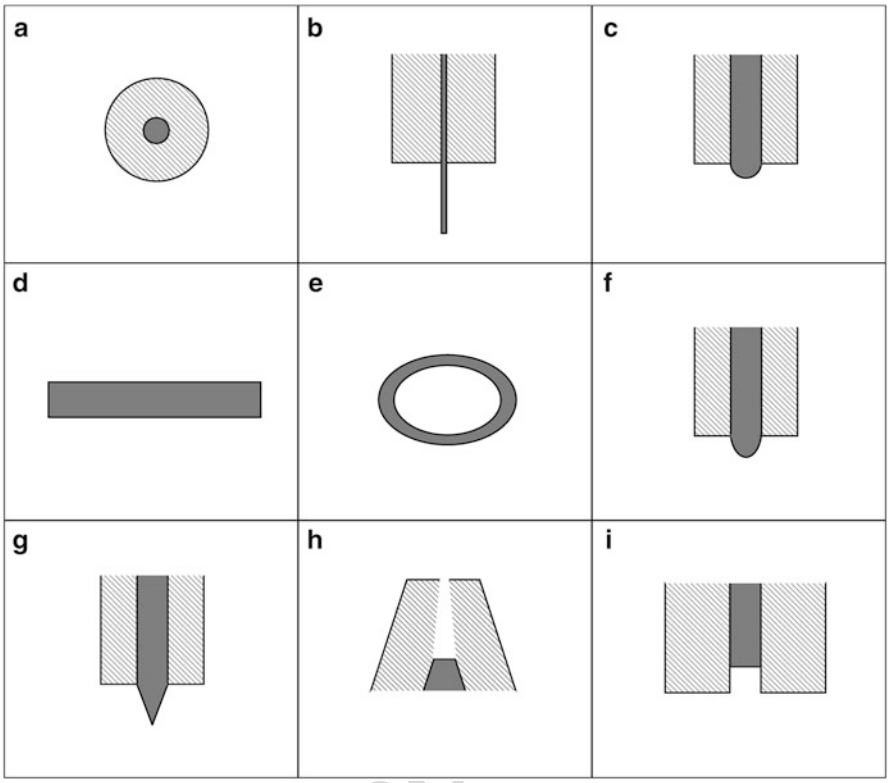

Fig. 15.5 Microelectrode configurations: (**a**) disk, (**b**) cylinder, (**c**) hemisphere, (**d**) band, (**e**) ring, (**f**) sphere caps, (**g**) cone, (**h**) nanopore, and (**i**) recessed microelectrode

15.3.1 Diffusion-Controlled Current-Time Responses for Application of a Potential Step

Spherical and hemispherical microelectrodes are the simplest cases, as the diffusion equation is T1,2, i.e., same as that described for conventional spherical electrodes. Thus, the first term (i.e., the Cottrell equation) dominates at short times, where the diffusion layer is thin with respect to the electrode radius. At longer times, the second term dominates and the diffusion layer grows much larger than r_0.

Many applications of MEs are based on steady-state currents, and therefore Table 15.2 shows the equations that predict steady-state currents for both spherical and hemispherical MEs (T2,2 and T2,3, respectively). Moreover, an equation has been derived that allows establishing the time (t_ε) needed to achieve a steady state within a ε % closeness for a spherical ME[2]:

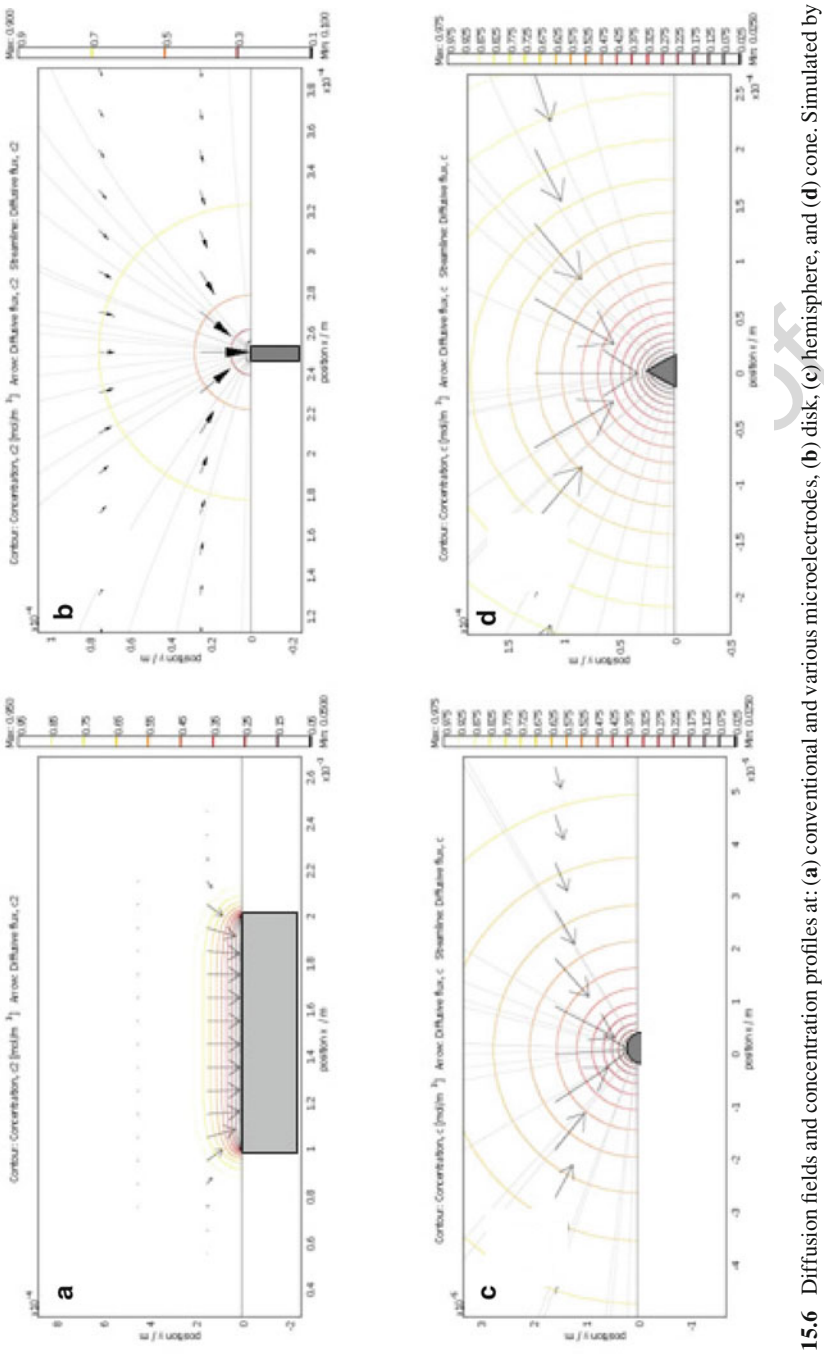

Fig. 15.6 Diffusion fields and concentration profiles at: (**a**) conventional and various microelectrodes, (**b**) disk, (**c**) hemisphere, and (**d**) cone. Simulated by the use of COMSOL Multiphysics 3.5

t.1 **Table 15.2** Current-time and long-time equation for different geometries

t.2 Microelectrode geometry	Current-time equation		Long-time equation	
t.3 Sphere, hemisphere	$i = \frac{nFAD_o^{1/2} \cdot C_o^*}{\pi^{1/2} t^{1/2}} + \frac{nFAD_oC_o^*}{r_o}$	$T_{2,1}$	$i = 4\pi nFD_oC_o^*r_o$	$T_{2,2}$
t.4			$i = 2\pi nFD_oC_o^*r_o$	$T_{2,3}$
t.5 Microdisk	$i(\tau) = \frac{4nFAD_oC_o^*}{\pi \cdot r_o} f(\tau)$	$T_{2,4}$	$i = 4nFD_oC_o^*r_o$	$T_{2,8}$
t.6	$\lim_{t\to 0} f(\tau) = \sqrt{\frac{\pi}{4\tau}} + \frac{\pi}{4} + \frac{3 \cdot \pi \cdot \tau}{2^{10}} + \ldots$	$T_{2,5}$		
t.7	$\lim_{t\to \infty} f(\tau) = 1 + \sqrt{\frac{16}{\pi^3 \cdot \tau}} + \ldots$	$T_{2,6}$		
t.8	$f(\tau) = 0.7854 + 0.8862 \cdot \tau^{-1/2} + 0.2146 \cdot e^{-0.7823 \cdot \tau^{-1/2}}$	$T_{2,7}$		
t.9 Cylinder	$i = \frac{nFAD_oC_o^*}{r_o}\left[\frac{2\exp(-0.05\pi^{1/2}\tau^{1/2})}{\pi^{1/2}\tau^{1/2}} + \frac{1}{\ln(5.2945 + 0.7493\tau^{1/2})}\right]$	$T_{2,9}$	$i = \frac{2nFAD_oC_o^*}{r_o \ln(4D_ot/r_o^2)}$	$T_{2,11}$
t.10	$\tau = 4D_ot/r_0^2$			
t.11	$i = \frac{nFAD_oC_o^*}{r_o}\left[\frac{1}{\sqrt{\pi\theta}} + 0.422 - 0.0675\log(\theta) \pm 0.0058\left[\log(\theta) - 1.47\right]^2\right]$	$T_{2,10}$		
t.12 Banding	$i = nFD_oC_o^*l\left\{(\pi\theta)^{-1/2} + 0.97 - 1.10\exp\left[\frac{-9.90}{\lvert\ln(12.37\theta)\rvert}\right]\right\}$	$T_{2,12}$	$i = \frac{2\pi nFAD_oC_o^*}{w\ln(64D_ot/w^2)}$	$T_{2,13}$
t.13	$\theta = D_ot/w^2$		$i = nFC_o^*D\frac{\pi(a+d)}{\ln 16(d+a)/(d-a)}$	$T_{2,14}$
t.14 Recessed electrode			$i = \frac{4\pi nFC_o^*Dr_o^2}{4L + \pi r}$	$T_{2,15}$
t.15 Pore electrode			$i = 4nFaD_oC_o^*\left[\frac{(1 + (d/a)\tan\vartheta)}{(4d/a\pi) + (1 + (d/a)\tan\vartheta)}\right]$	$T_{2,16}$

t.1 **Table 15.3** Estimate of the timescales where a pure Cottrell (a) behavior or a steady-state (b) response for various microsized spheres is attained

t.2 Diameter/μm	(a) Cottrell response	(b) Steady-state response
t.3 0.05	<2.5 ns	>0.4 ms
t.4 0.5	<0.25 ms	>40 ms
t.5 5	<25 μs	>4 s
t.6 50	<2.5 ms	>400 s

t.1 **Table 15.4** Mass transfer coefficient, $m_{0,}$ for some microelectrodes of different geometry

t.2 Band		Cylinder		Disk		Hemisphere		Sphere	
t.3 $\frac{2\pi Do}{wln(64D_o\tau/w^2)}$	$T_{3,1}$	$\frac{2D_o}{r_o ln\tau}$	$T_{3,2}$	$\frac{4D_o}{\pi r_o}$	$T_{3,3}$	$\frac{D_o}{r_o}$	$T_{3,4}$	$\frac{D_o}{r_o}$	$T_{3,5}$

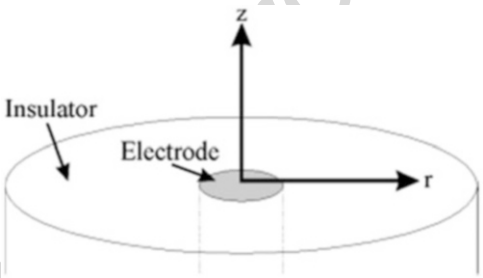

Fig. 15.7 Geometry of diffusion at a microdisk electrode

$$t_\varepsilon = 10^4 d^2/\left(\pi^3 D\varepsilon\right) \tag{15.14}$$

where d is the electrode diameter and D is the diffusion coefficient of the electroactive species. Table 15.3 shows examples of timescales estimated with an error of 5 % for various spherical MEs of different sizes, where the current follows the Cottrell or the steady-state behavior (Table 15.4). AU11

The microdisk (Fig. 15.7) is the most popular electrode for practical applications, as it can be fabricated easily, for instance, by encapsulating carbon fibers or metal wires in glass capillaries and then polishing the tips to expose the microdisk surfaces.[9, 13] However, theory is complicated because diffusion occurs in two dimensions, either normal to the electrode plane (z-axis) or radially (r direction) with respect to the axis of symmetry (Fig. 15.7). As a consequence, the current density is not uniform across the electrode surface, it being larger at the edge. The diffusion equation for this geometry is written in cylindrical coordinates (T1,4 in Table 15.1). This choice allows to account for the behavior of the disk ME either at short times, where the diffusion layer is almost parallel to the electrode surface, except to the edge, and z becomes the predominant variable, or at long times, where the diffusion layer grows to a hemi-circle, and it is accounted for the radial coordinate that becomes predominant.

The solution of equation T1,4 is not easy and, therefore, approximate analytical solutions have been derived. The analytical expressions derived by Aoki and Osteryoung and, later on, by Shoup and Szabo (equations T2,4–6 and T2,7, respectively, in Table 15.2) are commonly employed for practical applications. They contain the parameter, τ, that can be regarded as a dimensionless time:

$$\tau = \frac{4D_0 t}{a^2}$$

where a is the microdisk radius. The function $f(\tau)$ in equation T2,4 assumes two forms for large (i.e., $\tau > 1$) or small (i.e., $\tau < 1$) values of τ and corresponds to long or short times, respectively. It was also verified that the two curves overlap in the domain: $0.82 < \tau < 1.44$. More convenient is the single expression T2,7, which covers the entire range of τ. From these equations two limiting forms, as for spherical microelectrodes, can be derived for t (or τ) $\rightarrow 0$ and t (or τ) $\rightarrow \infty$. At short times equations T2,5 and T2,7 reduce to the Cottrell relationship, while at long times, equations T2,5 and T2,7 converge to a steady-state current given by T2,8. It is useful to mention that the latter result for the microdisk was derived first by Saito by the method of the Bessel expansion.[17]

By analogy to the rigorous result for the spherical microelectrodes and in view of the same functional form, it is possible to estimate the current at microdisks, over a large timescale range, as the combination of the Cottrell and the steady-state terms:

$$i_t = \frac{nFAD_O^{\frac{1}{2}} \cdot C_O^*}{\pi^{\frac{1}{2}} t^{\frac{1}{2}}} + 4nFD_O C_O^* a \qquad (15.15)$$

This approximate relationship is accurate at the short- and long-time regimes, while it deviates from the results reported by Aoki and Osteryoung by only a few percent at intermediate-time regimes. The largest error of 7 % occurs for electrolysis time corresponding at $\tau = 1$.

The cylindrical ME, as for the microsphere, involves only a single dimension of diffusion. The corresponding expression of Fick's second law is equation T1,3 (in Table 15.1), and its solution, with the boundary conditions as those employed for the spherical electrode, provides an integral that can be evaluated analytically for short and long times, whereas it must be integrated numerically for intermediate times[18] (Table 15.2, T2,10). This equation contains the parameter $\theta = Dt/r_0$ and is valid within 1 % error for $\theta < 10^6$. The $\pm$ in T2,10 denotes + for $log(\theta) \geq 1.47$ and $-$ for $log(\theta) < 1.47$.[18] A more practical approximate equation, which is valid within 1.3 % error at any time, has also been derived (equation T2,9 in Table 15.2).[19] This equation contains the parameter $\tau = 4Dt/{r_0}^2$ and, as it occurs for a sphere, it displays two limiting situations. In the short-time limit, T2,9 reduces to the Cottrell expression, as in this situation , the diffusion layer thickness is small compared to the curvature of the electrode. In particular, for τ not larger than circa 0.01, the diffusion layer is not greater than ~10 % of r_0. In the long-time limit, the current can be predicted by equation T2,11, which still contains the parameter τ. Therefore,

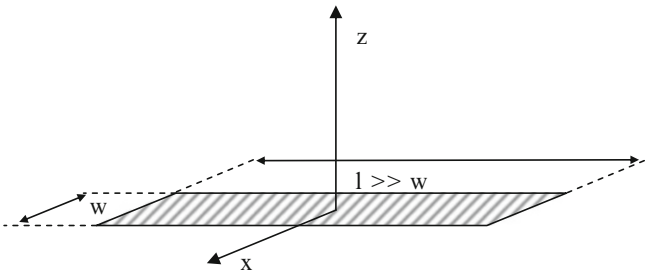

Fig. 15.8 Geometry of diffusion at a microband

it is not a steady state. However, the current shows a logarithmic dependence of the time and declines rather slowly, so that it assumes a quasi-steady state.

A band microelectrode is a two-dimensional diffusion system in which the length of the electrode is very much larger than the width. The coordinate system used to treat the diffusion problem at this geometry is shown in Fig. 15.8 and highlights that diffusion essentially occurs only along the x- and z-axes. This, as for the microdisks, causes the current density to be distributed nonuniformly and is especially infinite at the edge of the electrode.

Analytical expressions for the current-time curves have been derived for long and short times.[11] These are in the form of a series expansion, difficult to handle. A more convenient relationship that represents the two expansions as a closed form has also been derived (Table 15.2, T2,12). It contains the dimensionless parameter $\theta = Dt/w^2$, where w is the bandwidth and is valid for $\theta < 10^8$.[20, 21] Again, as it can now be expected, at short times, the current converges to the Cottrell equation; at long times the current approaches a limiting form, which, as for the cylindrical electrodes, contains the logarithmic dependence on t. Thus, also the band ME does not provide a true steady-state current at long times. An approximate, but simple, relationship for the long-time current has been derived by applying to the band ME an analogous treatment as for a hemicylinder.[19] In particular, it was noted that the current at a band of length l and width w was identical to that of a hemicylinder of length l and basal radius $r_0 = w/4$. This correspondence has provided the relationship T2,13 included in Table 15.2.

AU12

15.3.2 *Mass Transfer Coefficient*

As it has been discussed above, MEs display common features in the response of a potential step experiment, regardless of the geometry. At short times, where the diffusion layer is thin compared to the critical dimension of the ME, the current can be predicted by the Cottrell equation and planar diffusion is prevailing. At long times, where the diffusion layer is large compared to the critical dimension,

t.1 **Table 15.5** Voltammetric peak current for different electrode geometries

t.2 Electrode geometry	Peak (or maximum) current	
t.3 Microdisk	$i = 4nFD_oC_o^*a\left[0.34\exp(-0.66p) + 0.66 - 0.13\exp\left(-\frac{11}{p}\right) + 0.351p\right]$ $p = (nFa^2v/RTD_o)^{1/2}$	$T_{4,1}$
t.4 Microcylinder	$i = \frac{n^2F^2C_o^*Ar_ov}{RT}\left(\frac{0.446}{p} + \frac{0.335}{p^{1.85}}\right)$ $p = (nFr_o^2v/RTD_o)^{1/2}$	$T_{4,2}$
t.5 Microband	$i = nFC_o^*Dl\left[0.439p + 0.713p^{0.108} + \frac{0.614p}{1 + 10.9p^2}\right]$ $p = (nFw^2v/RTD_o)^{1/2}$	$T_{4,3}$

the current is steady state or quasi-steady state. Under the latter conditions, the current at the MEs is related to the mass transport coefficient, m_0, through

$$i = nFm_0C_O^*$$

The mass transfer coefficient m_0 represents the diffusion rate at the electrode surface and depends on the geometry as is shown in Table 15.5 for some of the MEs considered above. Thus, as can be easily inferred from the latter in the table, for extremely small electrodes, as is the case of NEs, the diffusion rate, and consequently, the current density, can be extraordinarily high.

15.3.3 Current-Potential Responses at ME

MEs in LSV or CV produce the same phenomena as in the potential step experiments. In these techniques, the transition from planar to radial diffusion, for a given ME and electrode geometry, is achieved by reducing the scan rate. The faster the transition, the smaller the characteristic length of the ME. Figure 15.9 shows, for instance, a series of CVs obtained at a microdisk electrode at different scan rates. It is evident that at high v, the CV displays the peak-shaped voltammogram as for planar electrodes; as the scan rate decreases, the CV becomes sigmoidal with the forward and backward curves retracing one another. This is caused by the formation of a stationary diffusion layer that is due to the high diffusion mass transport. The current at the stationary state is essentially independent of scan rate and the diffusion-limited current corresponds to that evaluated by a large potential step experiment described above. Theoretical modeling of the current-potential profiles at microelectrodes is usually difficult, and because of the complexity of the task, numerical solutions or digital simulation procedures have often been used. The only exception is the case of the spherical microelectrodes for which Eq. (12) can be applied.

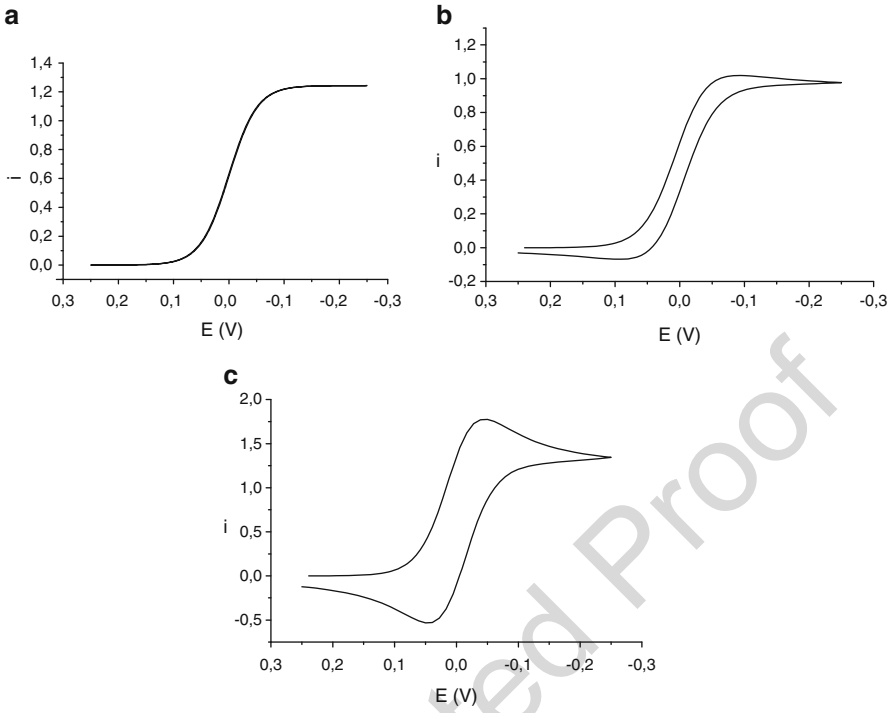

Fig. 15.9 Simulated CVs for a microdisk 12.5 μm radius at different scan rates: (**a**) $1 mVs^{-1}$; (**b**) $200 mVs^{-1}$; (**c**) $2 Vs^{-1}$

For disk,[22] cylinder,[23] and band[24] microelectrode geometries, theoretical expressions of the voltammograms have been derived as a function of the parameter, p, which contains the characteristic dimension of the specific ME. Since the peak or maximum current characterizes quantitatively the voltammograms, relevant expressions are given and shown in Table 15.4. In general, for large values of p, the equations $T_{4,1–3}$ are identical with the equation for planar diffusion. For small values of p, the latter equations approach those for the steady-state current displayed in Table 15.2 for the corresponding ME geometry.

15.3.4 Steady-State Current at Miscellaneous ME

In this section the relationships for steady-state current of various microelectrode of more complicated shapes are briefly described.

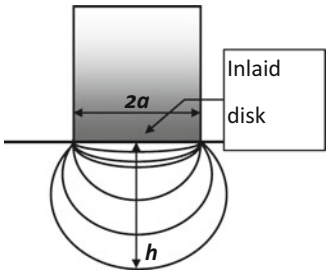

Fig. 15.10 Schematic view of a sphere-cap family of microelectrodes

15.3.4.1 Sphere Caps

Sphere caps are a family of microelectrodes that share a common basal plane of radius a and differ for the sphere-cap heights h (Fig. 15.10). A general expression that predicts the steady-state limiting current has been derived by numerical results and assumes the following form[25–27]:

$$i_d = \alpha(a,h)nFDc^b a \tag{15.16}$$

where $\alpha(a,h)$ is a shape-dependent factor that can be calculated by

$$\alpha(a,h) = 2\pi \int_0^\infty \frac{\cosh[x\arctan(h/a)]}{\cosh[x\arctan(a/h)]\cosh(\pi x/2)}dx \tag{15.17}$$

Because the latter equation is not easy to handle, an algebraic equation that fits Eq. (10) with good accuracy was sought. It was found the following simple relationship[28]:

$$\alpha(a,h) = 4 + \ln 10\left(\frac{h}{a}\right)^{1.36} \tag{15.18}$$

Equations (10) and (11) assume the values of 4 and 2π for the cases $h = 0$ (i.e., a microdisk) and $h = a$ (i.e., a hemisphere)[25–27], and, therefore, it exactly acquires the forms T2,2 and T2,3 for the microdisk and microhemisphere, respectively.

These kinds of microelectrodes can be prepared by cathodic deposition of mercury onto the surface of metal microdisks that are wettable by mercury. Details on their preparation and characterization can be found in references[25, 28].

15.3.5 Microring

The ring electrode can be fabricated as a cross section of an insulating rod on which metal is deposited in ultrathin film. The ring microelectrode can also achieve a

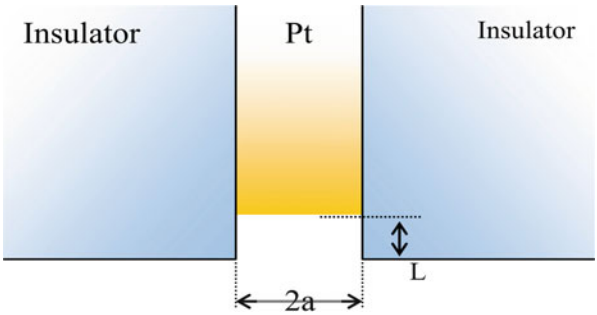

Fig. 15.11 Schematic view of a recessed microelectrode

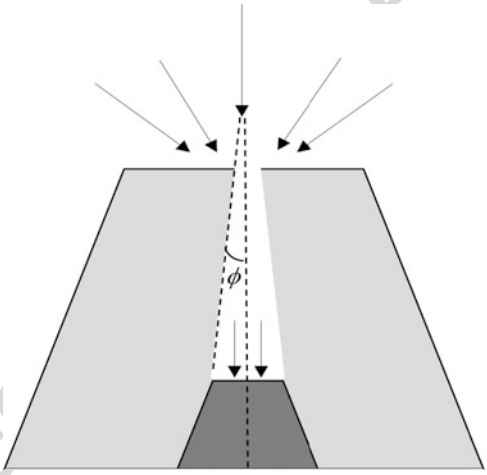

Fig. 15.12 Schematic view of a recessed microelectrode

steady state and supports large average current densities. However, as for the disk, it is characterized by nonuniform current density.[29–31] The steady-state current at the ring with an inner radius *a* and outer radius d is given by equation T2,14 in Table 15.2. Since the current varies slightly with the thickness of the ring, it depends almost on the radii rather than on the electrode area.

15.3.5.1 Recessed Microelectrodes and Nanopore Electrodes

In the recessed electrode, the active surface is located at the bottom of a hole. Simple geometry of the electrode is a disk as is shown in Fig. 15.11. These electrodes can be fabricated by etching the metal wires. The steady-state current for such geometry is expressed by equation T2,15.[32]

A geometry that is somewhat similar to recessed ME is that of the nanopore electrode (Fig. 15.12). This electrode geometry is characterized by the small pore orifice, whose radius, *a*, can be varied between 5 nm and 1 μm; the pore depth, *d*; and the half-cone angle ϕ. An approximate analytical expression for the steady-state limiting current is given by equation T2,16 in Table 15.2.[33]

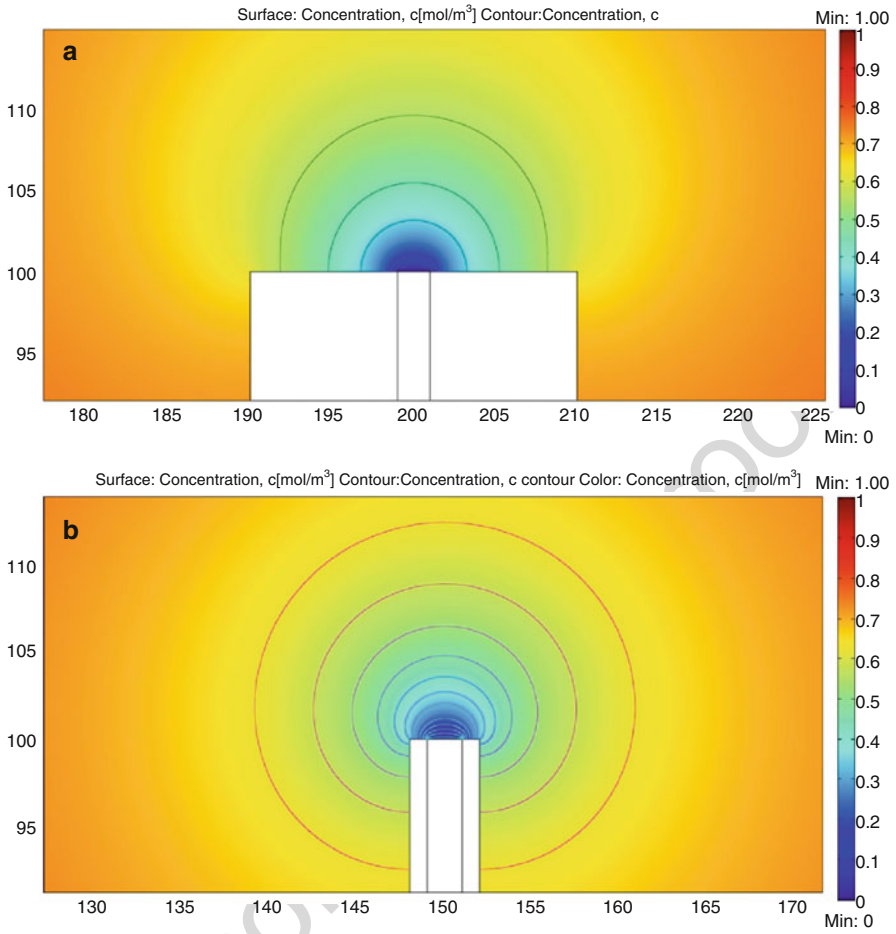

Fig. 15.13 Diffusion fields and concentration profiles at: (**a**) disk microelectrode RG → ∞; (**b**) RG → 1. Simulated by the use of COMSOL Multiphysics 3.5

15.3.5.2 Microelectrodes with Thin Shields

The interest for microelectrodes in which the insulating shields is of thickness comparable to the electrode radius is largely driven by the use of microelectrodes as tips in scanning electrochemical microscopy (SECM).[34, 35] One of the characteristic features of a thin-shielded microelectrode (TSM), with respect to microelectrodes that rest on an infinite insulating plane (as those previously described), is that, on the timescale of standard voltammetric measurements, the radial diffusion is also established behind the plane of the electrode and shield (for instance, contrasts the case of a microdisk in Fig. 15.13). Under these conditions, the flux, and consequently the current, is enhanced to an extent that depends on the relative size of insulating shield and electrode radius (normally referred to as *RG*).

t.1 **Table 15.6** Steady-state limiting equations for microdisk electrode with thin shields

t.2 Equation	Reference	Iss for RG → *1*
t.3 $Iss = 1.000 + 0.234\ (RG)^{-1} + 0.255\ (RG)^{-2}$	[39]	1.489
t.4 $Iss = 1.000 + 0.379\ (RG)^{2.342}]$	[40]	1.379
t.5 $Iss = 1.000 + 0.1380\ (RG - 0.6723)^{-0.8686}$	[38]	1.364

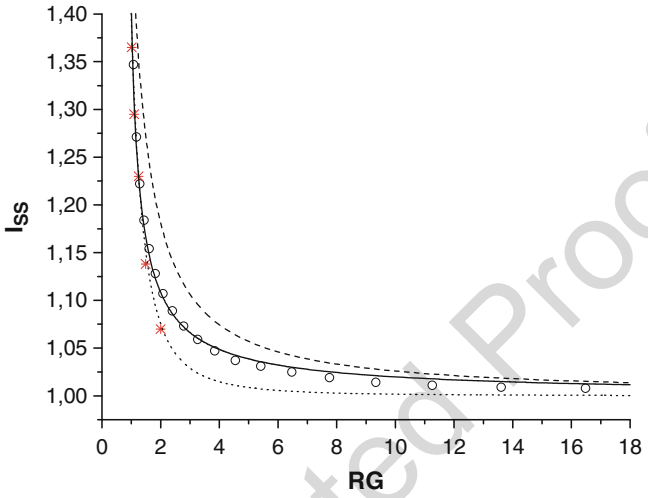

Fig. 15.14 Current against RG plot for a disk TMS: (*dashed lines*) from Ref. [39], (*dotted lines*) from Ref. [40], (*continuous line*) from Ref. [38], (*asterisk*) calculated from Ref. [36], (*open circle*) simulated from Ref. [41]

439 Equations for the steady-state limiting currents for such geometry are described in
440 this section for the case of the disk (Fig. 15.5a), sphere caps (Fig. 15.5f), and cone
441 (Fig. 15.5g).

442 Shoup and Szabo were the first to demonstrate, from a theoretical point of view,
443 that at TSMs diffusion from behind the plane of the electrode enhances the flux to
444 the inlaid disk.[36] This has also been confirmed by other researchers, who employed
445 different digital simulation procedures to obtain either steady-state limiting cur-
446 rents[37, 38] or cyclic voltammograms[39] for TSMs with a range of *RG*. From the
447 simulation data, approximate analytical expressions for the steady-state limiting
448 current (i_{ss}) as a function of *RG* have also been derived.[38–41] Table 15.6 summarizes AU13
449 such equations (in a dimensionless form, i.e., $I_{ss} = i_{ss}/i_d$) and the limiting current
450 values calculated for $RG \rightarrow 1$, while Fig. 15.14 displays either the graphical form of
451 the latter equations over a wide *RG* range or currents at discrete *RG* values[(36)].

452 For the sphere caps and cone geometries, more complex equations apply. The
453 diffusion problems to these geometries have been addressed by digital simulations,
454 and, therefore, only approximate solutions have been provided. Figure 15.15 shows
455 the parameters involved in the sphere-cap electrode. A general equation that links
456 all parameters involved in this geometry is[41]

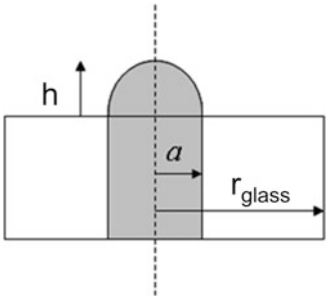

Fig. 15.15 Scheme of a sphere-cap geometry, $RG = r_{glass}/a$

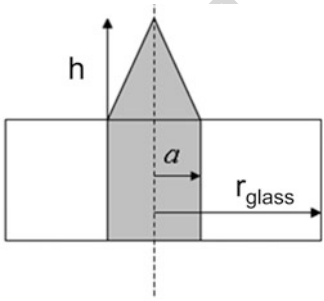

Fig. 15.16 Scheme of a cone geometry. $RG = r_{glass}/a$

$$I_{ss}^{sph} = \frac{1}{4}\Big[4 + 0.5780(RG - 0.6734)^{-0.8348} + \\ + \left(2.2832 + 9.3279(RG + 1.0321)^{-2-2979}\right) \cdot \left(\frac{h^{sph}}{a}\right)^{1.3590}\Big] \tag{15.19}$$

where

$$I_{ss}^{sph} = \frac{i_{ss}}{i_d} \tag{15.20}$$

and i_d stands for steady-state limiting current at a microdisk (i.e., equation T2,8 in Table 15.2)

For the micro-cone (see scheme of the geometry in Fig. 15.16), the following relationship has been derived[38]:

$$I_{ss}{}^{cono} = A + B(RG - C)^D \tag{15.21}$$

where the parameters A, B, C, and D are numerical constants which depend on the h/a ratio, as indicated in the table below.

	$h^{cone}/a = 0.5$	$h^{cone}/a = 1$	$h^{cone}/a = 2$	$h^{cone}/a = 3$
A	1.1270	1.2979	1.6769	2.0585
B	0.1972	0.2795	0.5240	0.8910
C	0.5667	0.4506	0.1794	−0.1900
D	−0.9025	−0.9436	−0.9857	−1.0280

15.4 Applications of Microelectrodes

The unique properties of microelectrodes such as low ohmic drop, high faradaic to capacitive current ratios, rapid achievement of steady-state currents, requirements of only two-electrode electrochemical cells, and small volume samples[4–10, 42–62] are exploited in many fields, including environmental,[56, 57] food,[58] biomedical [59–61], and material science areas.[62]

In electroanalysis, the majority of measurements with microelectrodes are taken under steady-state conditions by using either chronoamperometry (CA), linear sweep (LSV), or cyclic voltammetry (CV).[13–15, 17] Moreover, to enhance sensitivity in the measurements, fast-scan voltammetry (FSV)[63] or accumulation of analytes onto the electrode surface is also performed in conjunction with stripping analysis (SA).[64] FSV has largely been developed for biological applications[63, 66] and employs scan rates up to kV s^{-1}. FSV is also used for the detection of various anions and cations on sub-millisecond timescales.[50, 67–70]

SA is probably one of the fields where microelectrodes find the largest number of applications.[42, 45–47, 64, 68–70] With this regard, the enhanced mass transport to the microelectrode surface by diffusion can obviate, in general, the need for convective mass transport during the pre-concentration step before stripping, while making current responses less affected by convective forces in flowing systems.[64] In fact, in quiescent solutions, a steady-state current is established in a relatively short time for microelectrodes with disk, shrouded hemisphere, and sphere-cap geometries.[7–9, 12] As is illustrated in the previous sections, at microelectrodes which are not small enough in all their dimensions, as is the case for cylinders and bands, the current response attains only a quasi-steady state, as the equations for their currents contain time-dependent terms, even at long times.[7–9, 12] The mass transport properties need to be considered when optimizing analytical procedures in order to achieve the best performance in terms of reproducibility and pre-concentration efficiency for trace element analysis.[64] Natural convection, which may arise during relatively lengthy pre-concentration step experiments, does not affect the stripping responses at disk and sphere-cap microelectrodes[64], whereas some effects were observed with microwires.[64]

Because ohmic drop has little influence on voltammetric responses, additional supporting electrolytes in the solutions are often unnecessary.[7–9, 12] This largely avoids contamination of real samples with external chemicals when ultra-trace

element analysis has to be performed thereby leaving existing chemical equilibria unaltered. Therefore, direct measurements of low-ionic-strength samples or resistive media and speciation measurements can be performed straightforwardly without the need for pretreatment.[71, 72]

The lack of sufficient electrolyte in the media, however, makes the dependence of current on the concentration of electroactive species nonlinear, and the interpretation of the results requires that the migrational component in the transport be considered[7]; several reports and reviews deal with the theoretical problems related to the modeling of steady-state voltammograms at microelectrodes without or with dilute supporting electrolyte.[74–78] Fundamental studies describing the combined effects of diffusion and migration at microelectrodes have provided greater understanding and facilitated the prediction of amperometric experimental responses in complex systems such as solutions of polyelectrolytes, large polymer molecules with one or more ionic groups per monomer unit, colloidal suspensions, and polymeric gels.[73] Moreover, migration coupled with homogenous equilibrium and voltammetry in undiluted liquid organic substances has also been investigated from both a theoretical and experimental point of view.[73, 76–78]

List of Symbols (not specified in the text)

A	Area
D_i	Diffusion coefficient of the species (i)
erfc	Error inverse function
F	Faraday constant
n	Stoichiometric number of electrons involved in an electrode reaction
R	Gas constant
Z_i	Charge on species i
ν	Kinematic viscosity
∇	Vector operator
ϕ	Electrostatic potential

References

1. Bard AJ, Zoski CG (2000) Voltammetry retrospective. Anal Chem 72:346A–352A
2. Bond AM, Oldham KB, Zoski CG (1989) Steady-state voltammetry. Anal Chim Acta 216:177–230
3. Bard AJ, Faulkner LR (2001) Electrochemical methods. Fundamentals and applications. Wiley, New York, NY
4. Dayton MA, Brown JC, Stutts KJ, Wightman RM (1980) Faradaic electrochemistry at microvoltammetric electrodes. Anal Chem 52:946–950
5. Wightman RM (1981) Anal Chem 53:1125A–1134A

6. Bond AB, Fleischmann M, Robinson J (1984) The construction and behavior of ultramicroelectrodes – investigations of novel electrochemical systems. J Electrochem Soc 131:C109–C109 AU15
7. Deakin MR, Wipf D, Wightman RM (1986) Ultramicroelectrodes. J Electrochem Soc 133: C135–C135
8. Fleischmann M, Pons S, Rolison DR, Schmidt PP (1987) Ultramicroelectrodes. Datatech Systems Inc., Morganton, NC, p 363
9. Montenegro MI, Queirós MA, Daschbach JL (1991) Microelectrodes: theory and applications. Kluwer, The Netherlands
10. Heinze J (1993) Ultramicroelectrodes in electrochemistry. Angew Chem Int Ed Engl 32:1268–1288
11. Aoki K (1993) Theory of ultramicroelectrodes. Electroanalysis 5:627–639
12. Stulik K, Amatore C, Holub K, Marecek V, Kutner W (2000) Microelectrodes. Definitions, characterization, and applications (technical report). Pure Appl Chem 72:1483–1492
13. Zoski CG (2002) Ultramicroelectrodes: design, fabrication, and characterization. Electroanalysis 14:1041–1051
14. Arrigan DWM (2004) Nanoelectrodes, nanoelectrode arrays and their applications. Analyst 129:1157–1165
15. Oja SM, Wood M, Zhang B (2013) Nanoscale electrochemistry. Anal Chem 85:473–486
16. Zoski CG (2007) Handbook of electrochemistry. cap 6, 156–260 AU16
17. Saito Y (1968) Theoretical study on the diffusion current at the stationary electrode of circular and narrow band types. Rev Polarogr 15:177–187
18. Aoki K, Honda K, Tokuda K, Matsuda H (1985) Voltammetry at microcylinder electrodes. Part (II): chronoamperometry. J Electroanal Chem 186:79–86
19. Szabo A, Cope DK, Tallan DE, Kovack PM, Wightman RM (1987) Chronoamperometric current at hemicylinder and band microelectrodes: theory and experiments. J Electroanal Chem 217:417–423
20. Aoki K, Honda K, Tokuda K, Matsuda H (1987) Derivation of an approximate equation for chronoamperometric curves at microband electrodes and its experimental verification. J Electroanal Chem 230:61–67
21. Coen S, Cope DK, Tallan DE (1986) Diffusion current at a band electrode by an integral equation method. J Electroanal Chem 215:29–48
22. Aoki K, Akimoto K, Tokuda K, Osteryoung J (1984) Linear sweep voltammetry at very small stationary disk electrodes. J Electroanal Chem 171:219–230
23. Aoki K, Honda K, Tokuda K, Matsuda K (1985) Voltammetry at microcylinder electrodes: part I. Linear sweep voltammetry. J Electroanal Chem 182:267–279
24. Aoki K, Tokuda K (1987) Linear sweep voltammetry at microband electrodes. J Electroanal Chem 237:163–170
25. Baldo MA, Daniele S, Corbetta M, Mazzocchin GA (1995) Performance of platinum-based spherical mercury microelectrodes in cyclic voltammetry and stripping analysis. Electroanalysis 7:980–986
26. Myland JC, Oldham KB (1990) Diffusion-limited currents at hemispheroidal microelectrode. J Electroanal Chem 288:1–14
27. Alfred LCR, Oldham KB (1996) Steady-state currents at sphere-cap microelectrodes and electrodes of related geometry. J Phys Chem 100:2170–2177
28. Daniele S, Bragato C, Baldo MA, Mazzocchin GA (2002) Effects of mercury ion concentration on the preparation of mercury deposits on platinum microdisk electrodes. Ann Chim 92:203–215
29. Szabo AJ (1987) Theory of the current at microelectrodes: application to ring electrodes. J Phys Chem 91:3108–3111
30. Fleishmann M, Pons S (1987) The behavior of microdisk and microring electrodes. J Electroanal Chem 222:107–115
31. Cope DK, Scott CH, Tallman DE (1990) Transient behavior at planar microelectrodes: diffusion current at ring electrodes by the integral equation method. J Electroanal Chem 285:49–69

32. Bond AM, Luscombe D, Oldham KB, Zoski CG (1988) A comparison of the chronoamperometric response at inlaid and recessed disc microelectrodes. J Electroanal Chem 249:1–14
33. Zhang B, Zhang Y, White HS (2006) Steady-state voltammetric response of the nanopore electrode. Anal Chem 78:477–483
34. Bard AJ, Fan FRF, Mirkin MV (1994) In: Bard AJ, Rubistein I (eds) Electroanalytical chemistry, vol. 18. Marcel Dekker, New York, pp 243–373
35. Bard AJ, Mirkin MV, (2001) Scanning electrochemical microscopy (eds). Marcel Dekker, NewYork
36. Shoup D, Szabo A (1984) Influence of insulation geometry on the current at microdisk electrodes. J Electroanal Chem 160:27–31
37. Amphlett JL, Denuault G (1998) Scanning electrochemical microscopy (SECM): an investigation of the effects of tip geometry on amperometric tip response. J Phys Chem B 102:9946–9951
38. Zoski CG, Mirkin MV (2002) Steady-state limiting currents at finite conical microelectrodes. Anal Chem 74:1986–1992
39. Fang Y, Leddy J (1995) Cyclic voltammetric responses for inlaid microdisks with shields of thickness comparable to the electrode radius: a simulation of reversible electrode kinetics. Anal Chem 67:1259–1270
40. Zhao G, Giolando DM, Kirchoff JR (1995) Chemical vapor deposition fabrication and characterization of silica-coated carbon fiber ultramicroelectrodes. Anal Chem 67:2592–2598
41. Daniele S, Ciani I, Batistel D (2008) Effect of the insulating shield thickness on the steady-state diffusion-limiting current of sphere cap microelectrodes. Anal Chem 80:253–259
42. Wehmeyer KR, Wightman RM (1985) Cyclic voltammetry and anodic stripping voltammetry with mercury ultramicroelectrodes. Anal Chem 57:1989–1993
43. Li LJ, Fleischmann M, Peter LM (1987) *In-situ* measurements of Pb^{2+} concentration in the lead-acid battery using mercury ultramicroelectrodes. Electrochim Acta 32:1585–1587
44. Daniele S, Baldo MA, Ugo P, Mazzocchin GA (1989) Determination of heavy metals in real samples by anodic strypping voltammetry with mercury microelectrodes. Part 1. Application to wine. Anal Chim Acta 219:9–18
45. Daniele S, Baldo MA, Ugo P, Mazzocchin GA (1989) Determination of heavy metals in real samples by anodic stripping voltammetry with mercury microelectrodes. Part 2. Application to rain and sea waters. Anal Chim Acta 219:19–25
46. Daniele S, Baldo MA, Ugo P, Mazzocchin GA (1990) Voltammetric probe of milk samples by using a platinum microelectrode. Anal Chim Acta 238:357–366
47. Wojciechowski M, Balcerzak J (1991) Square-wave anodic stripping voltammetry of lead and cadmium at cylindrical graphite fiber microelectrodes with in situ plated mercury films. Anal Chim Acta 249:433–445
48. Stulik K (1989) Some aspects of flow electroanalysis. Analyst 114:1519–1525
49. La Course WR, Modi SJ (2005) Microelectrode applications of pulsed electrochemical detection. Electroanalysis 17:1141–1152
50. Harman AR, Baranski AS (1990) Fast cathodic stripping analysis with ultramicroelectrodes. Anal Chim Acta 239:35–44
51. Craston DH, Jones CP, Williams DE (1991) Microband electrodes fabricated by screen printing processes: applications in electroanalysis. Talanta 38:17–26
52. Farrington AM, Jagota N, Slater JM (1994) Simple solid wire microdisk electrodes for the determination of vitamin-C in fruit juices. Analyst 119:233–238
53. Bixler JW, Bond AM (1986) Amperometric detection of picomole samples in a microdisk electrochemical flow-jet cell with dilute supporting electrolyte. Anal Chem 58:2859–2863
54. Davis F, Higson SPJ (2013) Arrays of microelectrodes: technologies for environmental investigations. Environ Sci Process Impacts 15:1477–1489
55. Tan F, Metters JP, Banks CE (2013) Electroanalytical applications of screen printed microelectrode arrays. Sensor Actuator B 181:454–462

AU17

56. Pecková K, Barek J (2011) Boron doped diamond microelectrodes and microelectrode arrays in organic electrochemistry. Curr Org Chem 15:3014–3028
57. Marinesco S, Frey O (2013) Microelectrode designs for oxidase-based biosensors. NeuroMethods 80:3–25
58. Sun X, Luo Y, Liao F, Lu W, Chang G (2011) Novel nanotextured microelectrodes: electrodeposition-based fabrication and their application to ultrasensitive nucleic acid detection. Electrochim Acta 56:2832–2836
59. Ordeig O, Del Campo J, Muñoz FX, Banks CE, Compton RG (2007) Electroanalysis utilizing amperometric microdisk electrode arrays. Electroanalysis 19:1973–1986
60. Li CM, Hu W (2013) Electroanalysis in micro- and nano-scales. J Electroanal Chem 688:20–31
61. Bunin MA, Wightman RM (1998) Quantitative evaluation of 5-hydroxytryptamine (serotonin) neuronal release and uptake: an investigation of extrasynaptic transmission. J Neurosci 18:4854–4860
62. Daniele S, Baldo MA, Bragato C (2008) Recent developments in stripping analysis. Curr Anal Chem 4:215–228
63. Molina A, Laborda E, Martínez-Ortiz F, Bradley DF, Schiffrin DJ, Compton RG (2011) Comparison between double pulse and multipulse differential techniques. J Electroanal Chem 659:12–24
64. Takmakov P, McKinney CJ, Carelli RM, Wightman RM (2011) Instrumentation for fast-scan cyclic voltammetry combined with electrophysiology for behavioral experiments in freely moving animals. Rev Sci Instrum 82 art 074302
65. Wood KM, Hashemi P (2013) Fast-scan cyclic voltammetry analysis of dynamic serotonin responses to acute escitalopram. ACS Chem Neurosci 4:715–720
66. Apulche-Aviles MA, Baur JE, Wipf DO (2008) Imaging of metal ion dissolution and electrodeposition by anodic stripping voltammetry-scanning electrochemical microscopy. Anal Chem 80:3612–3621
67. Munteanu G, Munteanu S, Wipf DO (2009) Rapid determination of zeptomole quantities of Pb^{2+} with the mercury monolayer carbon fiber electrode. J Electroanal Chem 632:177–183
68. Yang Y, Pathirathna P, Siriwardhane T, McElmurry SP, Hashemi P (2013) Real-time subsecond voltammetric analysis of Pb in aqueous environmental samples. Anal Chem 85:7535–7541
69. Sigg L, Black F, Buffle J, Cao J, Cleven R, Davison W, Galceran J, Gunkel P, Kalis E, Kistler D, Martin M, Noel S, Nur Y, Odzak N, Puy J, van Riemsdijk W, Temminghoff E, Tercier-Waeber ML, Toepperwien S, Town RM, Unsworth E, Warnken KW, Weng L, Xue H, Zhang H (2006) Comparison of analytical techniques for dynamic trace metal speciation in natural freshwaters. Environ Sci Technol 40:1934–1941
70. Buffle J, Tercier-Waeber ML (2005) Voltammetric environmental trace-metal analysis and speciation: from laboratory to in situ. Trends Anal Chem 24:172–191
71. Ciszkowska M, Stojek Z (1999) Voltammetry in solutions of low ionic strength. Electrochemical and analytical aspects. J Electroanal Chem 466:129–143
72. Daniele S, Mazzocchin GA (1993) Stripping analysis at mercury microelectrodes in the absence of supporting electrolyte. Anal Chim Acta 273:3–11
73. Peña MJ, Fleischmann M, Garrard N (1987) Voltammetric measurements with microelectrodes in low-conductivity systems. J Electroanal Chem 220:31–40
74. Oldham KB (1988) Theory of microelectrode voltammetry with little electrolyte. J Electroanal Chem 250:1–21
75. Oldham KB (1997) Limiting currents for steady-state electrolysis of an equilibrium mixture, with and without supporting inert electrolyte. Anal Chem 69:446–453
76. Daniele S, Baldo MA, Bragato C, Abdelsalam ME, Denuault G (2002) Steady-state voltammetry of hydroxide ion oxidation in aqueous solutions containing ammonia. Anal Chem 74:3290–3296

77. Xu X, Zhang S, Chen H, Kong J (2009) Integration of electrochemistry in micro-total analysis systems for biochemical assays: recent developments. Talanta 80:8–18
78. Zhang DA, Rand E, Marsh M, Andrews RJ, Lee KH, Meyyappan M, Koehne JE (2013) Carbon nanofiber electrode for neurochemical monitoring. Mol Neurobiol 48:380–385
79. Jaquins-Gerstl A, Michael AC (2013) The advantage of microelectrode technologies for measurement in delicate biological environments such as brain tissue. NeuroMethods 80:55–68
80. Prehn R, Abad L, Sánchez-Molas D, Duch M, Sabaté N, Del Campo FJ, Muñoz FX, Compton RG (2011) Microfabrication and characterization of cylinder micropillar array electrodes. J Electroanal Chem 662:361–370
81. Godino N, Borrise X, Muñoz FX, Del Campo FJ, Compton RG (2009) Mass transport to nanoelectrode arrays and limitations of the diffusion domain approach: theory and experiment. J Phys Chem C 113:11119–11125
82. Li LJ, Hawkins M, Pons JW, Daschbach J, Pons S, Fleischmann M, Abrantes LM (1989) The behavior of microdisk and microring electrodes – the chronoamperometric response at microdisk and microring electrodes. J Electroanal Chem 262:45–53
83. Oldham KB (1981) Edge effects in semiinfinite diffusion. J Electroanal Chem 122:1–17

Author Queries

Chapter No.: 15 307792_1_En

Query Refs.	Details Required	Author's response
AU1	Please check whether the affiliation of the authors are appropriate as typeset.	
AU2	Please check whether the cross reference inserted for Chap. 2.4 is Ok.	
AU3	Note that equations are converted from picture format. Please check whether all the equations are presented appropriately throughtout the chapter.	
AU4	Note that equations are renumbered. Please check whether the cross references are appropriate and provide citations for the following cross references:(Eq. 15.12) in the sentence "The only exception is. . ."(Eq. 15.10) in the sentence "Because the latter equation. . ."(Equations 15.10 and 15.11) in the sentence "Equations (15.10) and (15.11) assume the values. . ."	
AU5	Please check whether the headings are assigned to their appropriate section levels.	
AU6	Note that cross references for inline equations in tables (e.g., equation T1,3) have been retained as in manuscript throughout the chapter. Please check and renumber if necessary.	
AU7	Please check whether the presentation of data in all tables is appropriate.	
AU8	Note that texts inside the Artworks of Figs 15.3 and 15.6 are not clear. Please provide better quality image.	
AU9	Note that numbering of equations in tables are mentioned in superscript form (e.g., T1,3), while both inline and superscript forms are found in the text citations. Please make it consistent.	

AU10	Please check if sentence starting "The time needed…" should be deleted as this is a repetition of previous sentence.	
AU11	Note that citation for Table 15.4 has been inserted after the para "Table 15.3 shows examples of time-scales…" for sequential order of citations. Please check.	
AU12	Please check if "bandwidth" is okay as edited.	
AU13	Please check if edit to the latter part of sentence starting "Table 15.6 summarizes …" is okay.	
AU14	Note that refs. [65, 79, 80–83] are not cited in the text. Please cite the references in text or delete them from the list.	
AU15	Please provide article title for ref. [5].	
AU16	Please provide complete bibliographic details for ref. [16] if possible.	
AU17	Please provide complete bibliographic details for refs. [34, 35].	